IOP PUBLISHING JOURNAL OF PHYSICS D: APPLIED PHYSICS

J. Phys. D: Appl. Phys. **46** (2013) 135106 (7pp) doi:10.1088/0022-3727/46/13/135106

Quantum theory of operation for rectenna solar cells

Sachit Grover[1], **Saumil Joshi and Garret Moddel**

Department of Electrical, Computer, and Energy Engineering, University of Colorado, Boulder, CO 80309-0425, USA

E-mail: sachitgrover@ieee.org

Received 7 November 2012, in final form 6 February 2013
Published 5 March 2013
Online at stacks.iop.org/JPhysD/46/135106

Abstract

Optical rectennas, sub-micrometre antenna-coupled diodes, can directly rectify solar and thermal electromagnetic radiation, and have been proposed as an alternative to conventional semiconductor photovoltaics. We develop a comprehensive description of the operating principle of rectenna solar cells. In prior work classical concepts from microwave rectenna theory have been applied to the analysis of photovoltaic power generation using these ultra-high frequency rectifiers. Because of their high photon energy the interaction of petahertz frequency waves with fast-responding diodes requires a semiclassical analysis. We use the theory of photon-assisted transport to derive the current–voltage [$I(V)$] characteristics of metal/insulator/metal tunnel diodes under illumination. We show how power is generated in the second quadrant of the $I(V)$ characteristic, derive solar cell parameters, and analyse the key variables that influence the performance under monochromatic radiation and to a first order approximation. The efficiency improves with reduced dark current under reverse bias and increasing incident electromagnetic power.

(Some figures may appear in colour only in the online journal)

1. Introduction

A rectenna [1] is a high-frequency rectifier system consisting of an antenna that receives electromagnetic radiation and a diode that converts it to dc power. The main application for rectennas has been infrared sensing and detection [2–4]. Even though the concept of solar rectification was first proposed in the 1970s [5] active research on rectennas for solar energy harvesting has gathered momentum only recently [6–9]. Harvesting solar or thermal energy using optical frequency rectennas is a potential low-cost route to high-efficiency photovoltaics. The materials are inexpensive and not limited in availability, and the fabrication is suited to roll-to-roll manufacturing [10]. Semiconductor solar cells are fundamentally limited in the minimum frequency of radiation that can be harvested being proportional to the bandgap [11]. A rectenna's frequency response is dependent primarily on the design of the antenna [12] and its impedance match to the diode [13]. Femtosecond-fast metal/insulator/metal tunnel diodes [6, 14–16], as well as new low-capacitance and low-resistance geometric diodes [17] are being considered as potential rectifiers for efficient rectennas. While significant experimental work is underway to find appropriate diodes, a comprehensive understanding of optical rectenna physics is lacking.

Previous estimates of rectenna efficiency extended microwave concepts [18] to optical frequencies [16, 19–21] by analysing a classical circuit model using resistance and responsivity of the diode, but this analysis for classical rectifier is valid only at a sub-optical frequencies [6]. A semiclassical quantum-mechanical analysis of the diode characteristics is required for incident radiation at energy $\hbar\omega$ exceeding the electronic charge (e) times the voltage scale of the nonlinearity in the diode ($=eV_{\text{nonlinear}}$) [22, 23]. For simple comparison with voltage, we define photon voltage as $V_{\text{ph}} = \hbar\omega/e$. At these high frequencies, the energy of the incident photons affects the charge transport mechanism of the diode under illumination [24]. One way to include the quantum nature of electrons interacting with a high frequency signal is to use semiclassical values for the resistance and the responsivity, derived from the theory of photon-assisted transport (PAT), in the circuit model [13, 25, 26]. This is a viable approach

[1] Present address: National Center of Photovoltaics, National Renewable Energy Lab., Golden, CO 80401, USA.

for finding the quantum efficiency (QE) of the rectenna but a very indirect one for deriving the solar cell characteristics. We implement a straightforward alternative by extending PAT analysis to obtain a current–voltage $I(V)$ curve for the rectenna under illumination. The development of an $I(V)$ curve under illumination puts rectenna solar cells in the same perspective as conventional solar cells allowing for easy comparison of solar cell characteristics and performance. Moreover, it bridges the gap between the dark $I(V)$ of the diode and its performance under illumination allowing for a more accurate description and analysis than classical methods.

In PAT the electronic properties of a device are a function of the interactions of photons with electrons, which can be analysed using several approaches [27–30]. Here, we follow the derivation given by Tien and Gordon [22] for a superconducting junction and generalized for tunnel devices by Tucker *et al* [31]. In section 2, we give a summary of the salient features of PAT, also referred to here as the semiclassical theory, and its extension to the response of tunnel diodes under illumination. In section 3, we use the examples of piecewise linear and exponential static $I(V)$ curves to calculate $I(V)$ characteristics under monochromatic light. We also examine the power-conversion-efficiency limitation of rectennas. In section 4, we extend the analysis of the piecewise linear model to more realistic diodes that have a significant leakage in reverse bias. The effect of reverse bias leakage on efficiency and open circuit voltage is discussed.

2. Photon-assisted transport

The frequency at which classical circuit theory is no longer valid is $eV_{\text{nonlinear}}/\hbar$, as discussed above. For the superconducting diodes investigated by Dayem and Martin [24], $V_{\text{nonlinear}}$ corresponds to the bandgap energy of metal superconductors, on the order of 0.1 meV, corresponding to microwave frequencies. For optical frequencies, the relevant energy scale is greater than 100 meV, which corresponds to the $V_{\text{nonlinear}}$ in low-barrier metal/insulator/metal (MIM diodes) used in rectennas [32], and is related to the metal-insulator barrier height [31].

Consider the combination of an ac signal of amplitude V_ω at a frequency ω and a dc voltage V_{D} applied across the diode as

$$V_{\text{diode}} = V_{\text{D}} + V_\omega \cos(\omega t). \tag{1}$$

From a classical perspective, the effect of the ac signal can be visualized as modulating the Fermi level on one side of the tunnel junction while holding the other side at a fixed potential, as shown in figure 1. The resulting change in tunnelling distance causes a nonlinear excursion along the dc $I(V)$ curve around the bias point V_{D}.

In the semiclassical PAT theory, the effect of V_ω is accounted for through a time-dependent term in the Hamiltonian H for the contact [22], written as

$$H = H_0 + eV_\omega \cos(\omega t), \tag{2}$$

where H_0 is the unperturbed Hamiltonian in the contact. The corresponding unperturbed wavefunction is of the form

$$\psi(x, y, z, t) = f(x, y, z)\mathrm{e}^{-\mathrm{i}Et/\hbar}. \tag{3}$$

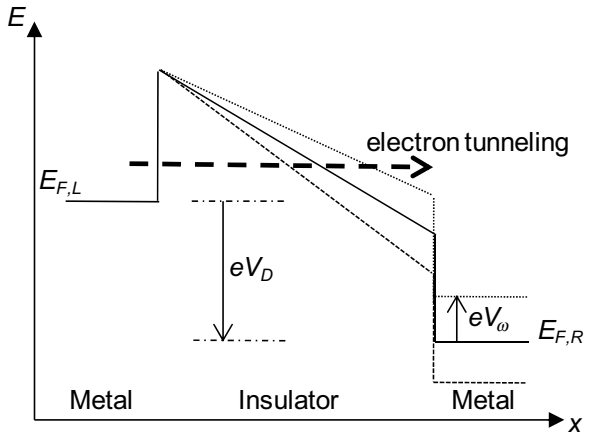

Figure 1. Classical model of the conduction band profile of an MIM diode modulated by an ac voltage. The metal Fermi levels are shown in the left and right hand regions of the curve, and the insulator conduction band edge is shown in the centre region. The ac signal causes the Fermi level difference between the left and right sides of the tunnel junction to oscillate causing a change in the tunnelling distance and thereby in the tunnel current.

The harmonic perturbation in equation (2) leads to an additional phase term whose effect is included in the wavefunction as

$$\psi(x, y, z, t) = f(x, y, z)\mathrm{e}^{-\mathrm{i}Et/\hbar} \times \exp\left[-(i/\hbar)\int^t \mathrm{d}t' eV_\omega \cos(\omega t')\right]. \tag{4}$$

Integrating the exponential over time and using the Jacobi–Anger expansion, the wavefunction in the contact is written as

$$\psi(x, y, z, t) = f(x, y, z)\sum_{n=-\infty}^{+\infty} J_n\left(\frac{eV_\omega}{\hbar\omega}\right)\mathrm{e}^{-\mathrm{i}(E+n\hbar\omega)t/\hbar}, \tag{5}$$

where J_n is the Bessel function of order n. The modified wavefunction indicates that electrons in the metal, previously located at energy E, can now exist at multiple virtual energy levels separated by the photon energy $\hbar\omega$, as shown in figure 2. The probability amplitude of the electron occupancy at energy $E \pm n\hbar\omega$ is given by the Bessel function of order n, where n corresponds to the number of photons absorbed or emitted by the electron in a multi-photon process. The time-dependent wavefunction is normalized since the infinite sum of the squares of Bessel terms is unity. The electron density is proportional to the modulus squared of the wavefunction and therefore to the square of the Bessel function.

A heuristic explanation for the effect of the wavefunction modulation on the tunnel current is based on the fact that all such single-electron states undergo the same modulation [23]. This implies that one can treat the problem in a first approximation as if, in addition to the dc voltage, there is a voltage nV_{ph} that is applied across the diode with a weighting factor $J_n^2(\alpha)$, where $\alpha = V_\omega/V_{\text{ph}}$. The dc current under illumination is then given by

$$I_{\text{illum}}(V_{\text{D}}, V_\omega) = \sum_{n=-\infty}^{\infty} J_n^2(\alpha) I_{\text{dark}}(V_{\text{D}} + nV_{\text{ph}}), \tag{6}$$

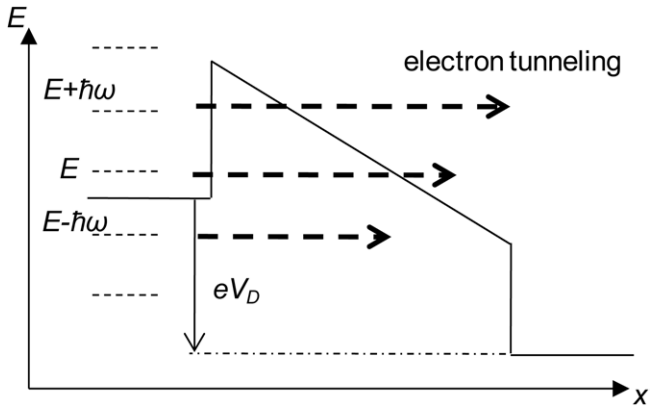

Figure 2. Conduction band profile of an MIM diode with PAT. The semiclassical theory gives the probabilities for electrons at energy E to absorb or emit photons and thus occupy the multiple energy levels shown, which are separated by $\hbar\omega$. The transmission probability of the electrons increase at higher energies. For both figures 1 and 2 the applied voltage produces a difference between the right-hand and left-hand Fermi levels. For clarity the modulated level is shown on the right-hand side of figure 1 and the left-hand side of figure 2.

where $I_{\rm dark}(V)$ is the tunnel current in the un-illuminated diode.

A similar derivation exists for the current in a diode illuminated by several frequencies [23]. Here we restrict the analysis to a single frequency.

Apart from the dc component of the tunnel current given by equation (6), there is a time-dependent current which consists of the harmonics of ω. From a time-dependent formulation for the tunnel current under optical excitation [25], the first harmonic is given by

$$I_\omega = \sum_{n=-\infty}^{\infty} J_n(\alpha)[J_{n+1}(\alpha) + J_{n-1}(\alpha)]I_{\rm dark}(V_{\rm D} + nV_{\rm ph}). \quad (7)$$

From equations (6) and (7) one can calculate the ac resistance $R_{\rm D}^{\rm SC}$ and responsivity $\beta_i^{\rm SC}$ using the equations [23]

$$R_{\rm D}^{\rm SC} = \frac{V_\omega}{I_\omega}; \qquad \beta_i^{\rm SC} = \frac{\Delta I}{\frac{1}{2}V_\omega I_\omega}, \quad (8)$$

where the superscript SC denotes the use of the semiclassical PAT formulation. The ΔI is the incremental dc current due to the illumination and is given by $\Delta I = I_{\rm illum} - I_{\rm dark}$.

From here on we assume that $\alpha \ll 1$ such that Bessel function terms only up to first order in n are required, simplifying the analysis. The validity of this condition will be verified in section 3 by calculating α and showing that it is less than unity. Physically, the above assumption corresponds to a small probability for photon emission or absorption involving more than a single photon. Mathematically, this is verified by taking the ratio of the Bessel functions for any order n and $n+1$. Using the approximation for Bessel functions (for $\alpha \ll 1$) $J_0(\alpha) \approx 1 - \alpha^2/4$ and $J_{\pm n}(\alpha) \approx (\pm\alpha/2)^n/(n!)$, we see that the ratio of $J_{n+1}/J_n = \alpha/(n+1)$, which implies that higher order contributions are negligible. From equation (7), to first order in $n(= -1, 0, 1)$, $R_{\rm D}^{\rm SC}$ is given by [25]

$$R_{\rm D}^{\rm SC} = \frac{2V_{\rm ph}}{I_{\rm dark}(V_{\rm D}+V_{\rm ph}) - I_{\rm dark}(V_{\rm D}-V_{\rm ph})} \xrightarrow{\text{classical}} \frac{1}{I'}, \quad (9)$$

which, in the classical limit ($\hbar\omega \to 0$) leads to the differential resistance. We note that the semiclassical resistance is the reciprocal of the slope of a secant between two points in the $I(V)$ curve separated by $2V_{\rm ph}$ rather than the tangential slope at a single point for the classical case.

The semiclassical responsivity is similarly found from the first order approximation of equations (6) and (7), and is given by [25]

$$\beta_i^{\rm SC} = \frac{1}{V_{\rm ph}}\left[\frac{I_{\rm dark}(V_{\rm D}+V_{\rm ph}) - 2I_{\rm dark}(V_{\rm D}) + I_{\rm dark}(V_{\rm D}-V_{\rm ph})}{I_{\rm dark}(V_{\rm D}+V_{\rm ph}) - I_{\rm dark}(V_{\rm D}-V_{\rm ph})}\right] \xrightarrow{\text{classical}} \frac{1}{2}\frac{I''}{I'}. \quad (10)$$

As with equations (9), (10) in the limit of small photon energies leads to the classical formula, here for responsivity given by 1/2 the ratio of second derivative of current to the first derivative.

Classically, the diode resistance and responsivity are independent of frequency. In comparison, the semiclassical resistance is lower than the classical and decreases with increasing frequency resulting in a better antenna to diode coupling efficiency since the antenna impedance is usually smaller than the diode resistance [13]. At high frequencies, the semiclassical responsivity approaches its maximum possible value of $1/V_{\rm ph} = e/\hbar\omega$ corresponding to unity QE. This indicates that even a diode with a poor QE at low frequencies can be adequately efficient at high frequencies [13].

The remainder of this article is devoted to understanding the ramifications of the modified dc $I(V)$ characteristics under illumination, given by terms up to first order in equation (6). An implicit assumption of the PAT theory used here is that the reservoir charge distribution extends up to the junction region and that the applied field does not influence the charge distribution in the junction [30]. This is a valid approximation for tunnel diodes because there is a high concentration of electrons in the metals and a low concentration in the insulating tunnel barrier. The validation of this approach is given by the condition $\alpha \ll 1$, which ensures that the injected carrier density in the insulator is small. An expression similar to equation (6) but applicable even to non-tunnelling based diodes is derived elsewhere [33], making the results presented here more generally applicable than the specific case of MIM diodes used in the analysis of PAT.

3. Illuminated $I(V)$ characteristics of ideal diode

In this section we use the PAT theory to derive the illuminated $I(V)$ characteristics of ideal diodes, i.e. for the case of an illuminated rectenna. The power-generating regime is shown to occur in the second quadrant of the $I(V)$ curve and the maximum achievable conversion efficiency for monochromatic illumination is shown to be 100%. In section 3.1 we assume that a constant ac voltage is applied across the diode as the dc bias voltage is varied, while in section 3.2 we assume a constant incident power mode. The first case helps to develop the understanding of how an illuminated $I(V)$ curve can be obtained starting with dark $I(V)$ using equation (6). The second case of constant power

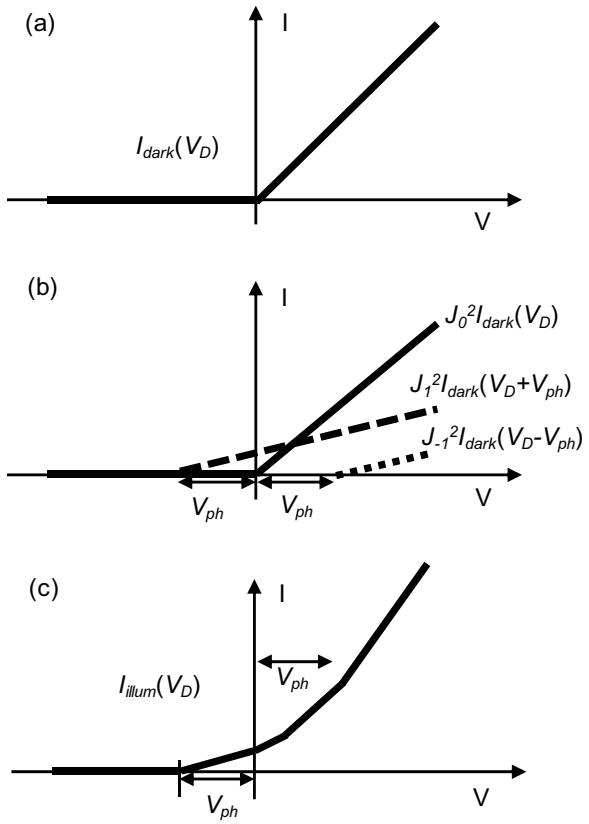

Figure 3. (*a*) Piecewise linear dark $I(V)$ curve. (*b*) Scaled and voltage-shifted components of $I_{\rm illum}$ as given by equation (11). (*c*) Illuminated $I(V)$ curve obtained by adding the components in (*b*). The region of positive current at negative voltage corresponds to power generation.

is closer to a practical situation in which the power incident from a source remains constant. Due to the dependence of the diode resistance on ac voltage as given by equation (9), the two assumptions lead to significantly different shapes of the illuminated $I(V)$ curves.

3.1. Constant ac voltage mode

Using the first order approximation of equation (6), corresponding to $\alpha \ll 1$, the current under illumination can be expressed as

$$I_{\rm illum}(V_{\rm D}) = \left(1 - \frac{\alpha^2}{4}\right)^2 I_{\rm dark}(V_{\rm D}) + \frac{\alpha^2}{4}(I_{\rm dark}(V_{\rm D} + V_{\rm ph}) + I_{\rm dark}(V_{\rm D} - V_{\rm ph})), \quad (11)$$

with the first term on the right-hand side representing the dark current due to electrons that are in the unexcited state. The second and the third terms represent the current resulting from electrons that undergo a net absorption or emission of a photon, respectively, together denoted as ΔI. To understand the effect of ΔI on $I_{\rm illum}$, consider an ideal diode with the piecewise linear $I_{\rm dark}$ shown in figure 3(*a*). As shown in figure 3(*b*), the two terms in ΔI modify $I_{\rm dark}$ such that a positive current can flow even at zero or a negative dc bias. The sum of the three current components of equation (11) is shown in figure 3(*c*) with power generation occurring in the second-quadrant operation of the diode. This is in contrast to the fourth-quadrant operation of a conventional solar cell. In a rectenna solar cell, the applied ac voltage generates a net photocurrent in the forward bias direction of diode. As in a battery or a generator, the internally produced positive current is sustained with a higher bias at the negative terminal leading to the second quadrant operation. The dc current generated depends on V_ω via α and thereby the strength of the illumination and the antenna design.

In the illuminated $I(V)$ curve shown in figure 3(*c*) the voltage-intercept is marked as $V_{\rm ph}$, which signifies the maximum negative voltage at which a positive current is possible. This occurs for a diode with a high forward-to-reverse current ratio.

3.2. Constant power mode

In the simplified representation given in section 3.1, we have assumed α and thereby V_ω to be constant with bias voltage $V_{\rm D}$. However, the resistance of the diode varies with $V_{\rm D}$ as given by equation (9). Therefore V_ω needs to be calculated as a function of $V_{\rm D}$ under constant illumination intensity when considering a complete rectenna circuit. We ignore losses in the antenna and assume perfect impedance matching between the antenna and diode for each $V_{\rm D}$. As the actual implementation of a rectifier would have a fixed operating point, the antenna and the impedance matching have to be designed only for that voltage.

Since the diode remains on throughout the ac cycle, the incident power is equal to the sum of ac $(1/2 V_\omega I_\omega)$ and dc $(-|V_{\rm D}\Delta I|)$ power dissipated in the diode and the rectified dc $(V_{\rm D}\Delta I)$ power available at the load, together given as

$$P_{\rm in} = P_{\rm diode} + |P_{\rm dc}| = \left\{-|V_{\rm D} I^{\omega}_{\rm DC}| + \frac{1}{2} V_\omega I_\omega + \text{harmonic loss}\right\} + |V_{\rm D} I^{\omega}_{\rm DC}| \approx \frac{1}{2} V_\omega I_\omega \approx \frac{V_\omega^2}{2 R_{\rm D}^{\rm SC}}. \quad (12)$$

Justification for the approximations is given below.

The above relation equates the incoming power to the ac power across the diode, its conversion to dc by the diode, and its subsequent transfer to the load. The modulus is used for $P_{\rm dc}$ to denote that the dc power generated in the diode is ultimately dissipated in the load. As discussed in section 2, only single photon excitations are produced at low intensities ($\alpha \ll 1$), as the higher harmonics are small as compared to the fundamental ac terms. Therefore the harmonic dissipation in the diode is negligible. For a given dark $I(V)$ curve we can substitute the $V_{\rm D}$ dependence of $R_{\rm D}^{\rm SC}$ from equation (9) in equation (12) and obtain V_ω as a function of $V_{\rm D}$ and $P_{\rm in}$.

In the case of no external load, the dc current is zero and all the input power is dissipated in the diode as ac loss. Under the condition that the dc resistance of the diode is much greater than the load resistance, this dissipation is primarily in the load and the dc power generated is most efficiently delivered to the load. The above condition is satisfied by a diode that has a negligible dark current under reverse bias, which is equivalent to the requirement for a high forward-to-reverse current ratio assumed in figure 3(*a*). The efficiency of the rectenna solar

cell in the bias voltage regime of $-V_{\rm ph} < V_{\rm D} < 0$ is given by

$$\eta = \frac{P_{\rm dc}}{P_{\rm in}} = |V_{\rm D}\beta_i^{\rm SC}|. \tag{13}$$

Under the first order approximation of equation (11), the largest absolute operating voltage of the rectenna for power generation in the second quadrant is $V_{\rm ph} = \hbar\omega/e$, while the maximum responsivity of the diode from equation (10) is $1/V_{\rm ph}$. Therefore the maximum theoretical value of η is unity. Power loss in the diode depends on the dc $I(V)$ characteristics as given in section 4. For the highly asymmetric ideal diode considered in this section, this loss is negligible.

For ideal dark $I(V)$ curves we calculate the illuminated $I(V)$ curves using equation (11) and find the maximum efficiency by dividing the product of dc power generated ($V_{\rm D} \times I_{\rm illum}$), with the fixed incident power ($P_{\rm in}$) used for calculating V_ω in equation (12). We perform this calculation for diodes with a low reverse leakage and a high forward-to-reverse current ratio using the piecewise linear model and an exponential model for the diode. The forward bias resistance (R_1) of the piecewise linear $I(V)$ curve is 100 Ω and the forward to reverse current ratio is $R_2/R_1 = 10^8$, where R_2 is the reverse bias resistance. The reverse saturation current of the exponential characteristics is 10^{-10} A and the logarithmic slope of the exponential $I(V)$ is 100 $\rm V^{-1}$. An input power of 10^{-8} W is assumed, at a photon energy of 1.5 eV. This power corresponds to the solar intensity of 100 mW $\rm cm^{-2}$ received over an area of 10 $\mu\rm m^2$. The $I(V)$ curves under illumination are given in figure 4(*a*) along with the efficiency of power conversion from ac to dc in figure 4(*b*) and the varying strength of the ac voltage source V_ω in figure 4(*c*). From the $I(V)$ curve in figure 4(*a*) we observe a negative open circuit voltage ($V_{\rm oc}$) and a positive short circuit current ($J_{\rm sc}$).

In the constant power mode, as the dc bias approaches $-V_{\rm ph}$ the semiclassical resistance increases leading to a sharp rise in V_ω as shown in figure 4(*c*). With V_ω and thereby α increasing, the slope of the first order terms in equation (11) increases leading to an abrupt knee in the light $I(V)$ curve as shown in figure 4(*a*). For a diode with a large reverse-bias resistance, the dark current loss at negative voltages is small leading to an almost rectangular $I(V)$ curve with the maximum efficiency occurring near $V_{\rm OC}$. As the negative bias exceeds $V_{\rm ph}$, the tunnelling electrons cannot access the empty states on the opposite side of the barrier with a single photon excitation. Thus under the first order approximation, the current drops to zero at $V_{\rm D} = -V_{\rm ph}$.

In a very small region near $V_{\rm D} \geqslant -V_{\rm ph}$, the first order approximation ($\alpha \ll 1$) breaks down. Nevertheless, in figure 4(*b*) we see that η for the piecewise linear model approaches unity at $V_{\rm D} > -V_{\rm ph}$. Therefore, under monochromatic illumination the power conversion efficiency does approach its maximum theoretical value of 100%.

For the near-ideal diodes considered here, the $I(V)$ curves under illumination are almost independent of the dark $I(V)$ curve. However, for non-ideal dark $I(V)$ curves, leakage under reverse bias decreases the fill-factor of the solar cell as shown in section 4.

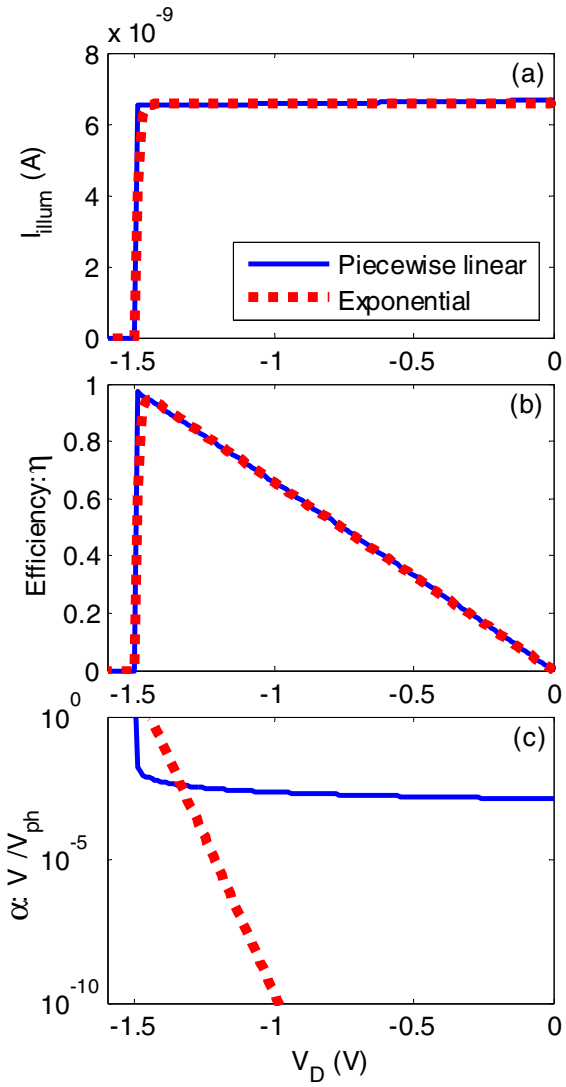

Figure 4. Device characteristics for a constant optical power supplied to the antenna. (*a*) Illuminated $I(V)$ characteristics for near-ideal piecewise-linear, and exponential dark $I(V)$ curves. (*b*) Efficiency given by the power delivered to the load (under the condition of a large diode resistance under reverse bias) divided by the total incident power ($P_{\rm in}$). (*c*) Argument of the Bessel function terms indicating the validity of the assumption that $\alpha \ll 1$ ($\alpha = V_\omega/V_{\rm ph}$ where $V_{\rm ph} = \hbar\omega/e$), and hence the approximation of including only first-order Bessel terms.

Several conclusions regarding rectification of monochromatic light can be drawn from the above results. Due to the rectangular illuminated $I(V)$ curve, the efficiency approaches a maximum value of 100% near an operating point of $V_{\rm D} = V_{\rm OC} = -V_{\rm ph}$. This is to be contrasted with figure 3, where the triangular illuminated $I(V)$, under the assumption of constant V_ω, incorrectly suggests a peak efficiency of only 25%. From figure 4(*a*) we verify that the product of $V_{\rm OC}I_{\rm SC}$ is equal to the input power of 10^{-8} W, consistent with solar cell characteristics. Broadband conversion efficiency is substantially lower [34].

In the above results, the efficiency increases as V_ω increases. This suggests that enhancing the ac field and thereby V_ω, by confining power in a small diode with a large resistance can lead to high efficiency [35]. This requires high impedance

antennas to match to the high impedance of the extremely confined diode structures, which might not be feasible with real antennas. Furthermore, the requirement for the diode *RC* time constant, independent of the diode size, to be smaller than the inverse of the frequency requires both the resistance and the capacitance of the diode to be small [13].

4. Illuminated $I(V)$ characteristics of real diodes

The illuminated $I(V)$ characteristics of a diode depend upon its dark characteristics. Here we obtain an analytical expression for the illuminated $I(V)$ curve using the simplified model of the piecewise linear dark diode. We then examine the performance of non-ideal diodes by varying the reverse leakage governed by R_2 and the power incident on the diode. The forward resistance R_1 is kept constant at 100 Ω. In the bias range of $-V_{ph} < V_D < 0$, we substitute the first-order approximation of equation (7) in equation (12), and assume $R_2/R_1 \gg 1$ to obtain

$$V_\omega = \sqrt{\frac{4P_{in}R_1}{(1+eV_D/V_{ph})}}. \quad (14)$$

The above equation gives the change in V_ω with dc bias as shown in figure 4(*c*). We substitute equation (14) in equation (11) to obtain the illuminated $I(V)$ curve

$$I_{illum}(V_D) = \frac{V_D}{R_2} + \frac{P_{in}}{E_{ph}/e}. \quad (15)$$

At $V_D = 0$ V, the above equation gives the expression for $I_{SC} = P_{in}/V_{ph}$. As seen in section 3, under the first order approximation the maximum achievable V_{OC} is $-V_{ph}$. To ensure $V_{OC} = -V_{ph}$, $I_{illum}(-V_{ph}) \geqslant 0$ requiring $R_2 \geqslant V_{ph}^2/P_{in}$. As shown in figure 5, the shape of the $I(V)$ curve under illumination is trapezoidal if $R_2 > V_{ph}^2/P_{in}$ and triangular if $R_2 < V_{ph}^2/P_{in}$. For an input power of 10^{-8} W and $V_{ph} = 1.5$ V, $V_{ph}^2/P_{in} = 2.25 \times 10^8$ Ω.

The reverse leakage current depends upon R_2 and determines the shape of the $I(V)$ and thereby the efficiency of a rectenna solar cell. In the triangular regime, the fill-factor is 25% and the efficiency is $0.25 \times P_{in}R_2/V_{ph}^2$. In the trapezoidal regime, the efficiency at the maximum power point is $1 - V_{ph}^2/P_{in}R_2$.

As seen in figure 5, an order of magnitude increase in R_2 causes the operating regime to change drastically leading to a sharp rise in efficiency. This reflects a critical balance between the reverse leakage and input power, in which the input power must provide a current that is much larger than the reverse leakage to maintain high efficiency. The expressions for efficiency are independent of R_1 as we have assumed a constant input power. Variations in R_1 would be compensated by a varying V_ω to keep the power constant. Under the first order approximation, the above results are valid only for small R_1 and $R_2/R_1 \gg 1$.

5. Conclusions

The operating mechanism of rectenna solar cells consisting of an optical antenna coupled to a diode is derived using the theory of photon-assisted transport. This mechanism is fundamentally different from the operating mechanism of semiconductor solar cells. Unlike conventional solar cells that provide power in the fourth quadrant of the $I(V)$ curve under illumination, rectenna solar cells operate in the second quadrant. The semiclassical form for the diode resistance equates the resistance at a bias to the inverse-slope of the secant between two points on the dark $I(V)$ curve separated by photon voltage from the bias. The nature of results derived is true for a more general nonlinear element than the specific case of MIM tunnel diodes used here [33].

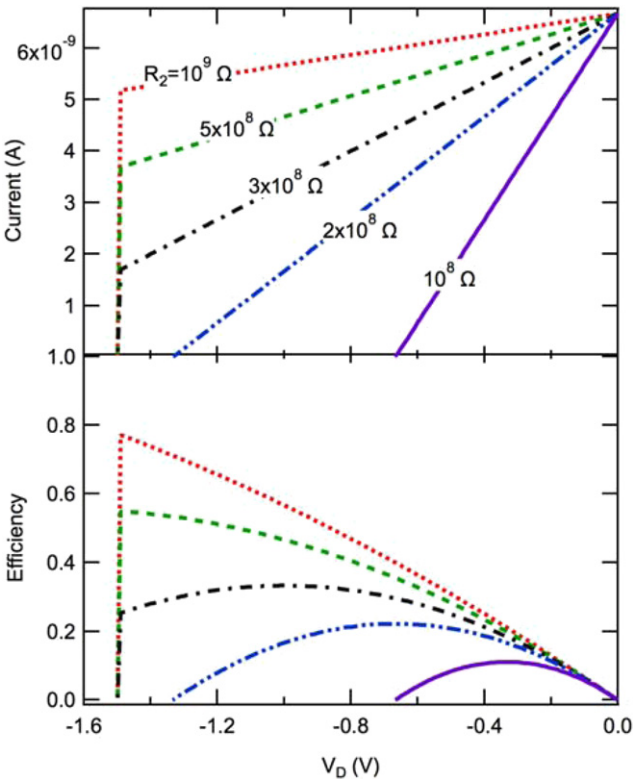

Figure 5. Illuminated $I(V)$ characteristics and efficiency curves for diodes with varying reverse leakage resistance, R_2. Slopes of the $I(V)$ curves are proportional to diode leakage under reverse bias and determine the efficiency of rectification. As the reverse leakage is reduced below a threshold ($R_2 > 2.25 \times 10^8$ Ω), the V_{OC} becomes equal to $-V_{ph} = -1.5$ V. The maximum power point also shifts towards $-V_{ph}$.

Due to the varying diode resistance with dc bias, the first-order semiclassical derivation for a single-frequency operation leads to a stepped $I(V)$ curve. For ideal diode characteristics this leads to a maximum achievable power conversion efficiency of rectenna solar cells near 100%, with a small amount of power lost as ac dissipation in the diode. The efficiency improves with increasing the diode asymmetry and the optical power. From an analytical expression for the light $I(V)$ curve corresponding to a piecewise linear diode, we observe that the reverse leakage resistance required for achieving high V_{OC} and hence high efficiency is inversely proportional to the optical power incident on the rectenna.

Acknowledgment

This work was carried out under contracts from Abengoa Solar and Hub Lab.

References

[1] Brown W C 1974 The technology and application of free-space power transmission by microwave beam *Proc. IEEE* **62** 11–24
[2] Michael Kale B 1985 Electron tunneling devices in optics *Opt. Eng.* **24** 242267
[3] Abdel-Rahman M R, Gonzalez F J, Zummo G, Middleton C F and Boreman G D 2004 Antenna-coupled MOM diodes for dual-band detection in MMW and LWIR *Proc. SPIE* **5410** 238–43
[4] Fumeaux C, Herrmann W, Kneubühl F K and Rothuizen H 1998 Nanometer thin-film Ni–NiO–Ni diodes for detection and mixing of 30 THz radiation *Infrared Phys. Technol.* **39** 123–83
[5] Bailey R L 1972 A proposed new concept for a solar-energy converter *J. Eng. Power* **94** 73
[6] Eliasson B J 2001 Metal–insulator–metal diodes for solar energy conversion *PhD Thesis* University of Colorado at Boulder, Boulder
[7] Corkish R, Green M A and Puzzer T 2002 Solar energy collection by antennas *Sol. Energy* **73** 395–401
[8] Goswami D Y, Vijayaraghavan S, Lu S and Tamm G 2004 New and emerging developments in solar energy *Sol. Energy* **76** 33–43
[9] Berland B 2003 Photovoltaic technologies beyond the horizon: optical rectenna solar cell *NREL Report* No SR-520-33263, Final Report 2003
[10] Kotter D K, Novack S D, Danis Slafer W and Pinhero P 2008 Solar nantenna electromagnetic collectors *ASME Conf. Proc.* **2008** 409–15
[11] Schockley W and Queisser H J 1961 Detailed balance limit of efficiency of pn junction solar cells *J. Appl. Phys.* **32** 510–9
[12] González F J and Boreman G D 2005 Comparison of dipole, bowtie, spiral and log-periodic IR antennas *Infrared Phys. Technol.* **46** 418–28
[13] Grover S and Moddel G 2011 Applicability of metal/insulator/metal (MIM) diodes to solar rectennas *IEEE J. Photovolt.* **1** 78–83
[14] Mayer A, Chung M S, Weiss B L, Miskovsky N M and Cutler P H 2010 Simulations of infrared and optical rectification by geometrically asymmetric metal–vacuum–metal junctions for applications in energy conversion devices *Nanotechnology* **21** 145204
[15] Choi K *et al* A focused asymmetric metal–insulator–metal tunneling diode: fabrication, DC characteristics and RF rectification analysis *IEEE Trans. Electron Devices* **58** 3519–28
[16] Osgood R M, Kimball B R and Carlson J 2007 Nanoantenna-coupled MIM nanodiodes for efficient vis/nir energy conversion *Proc. SPIE* **6652** 665203
[17] Zhu Z, Grover S, Krueger K and Moddel G 2011 Optical rentenna solar cells using graphene geometric diodes *37th IEEE PVSC* 002120–22
[18] Motjolopane B P and van Zyl R 2009 A review of rectenna models for electromagnetic energy harvesting *J. Eng. Des. Technol.* **7** 282–92
[19] Sanchez A, Davis C F Jr, Liu K C and Javan A 1978 The MOM tunneling diode: theoretical estimate of its performance at microwave and infrared frequencies *J. Appl. Phys.* **49** 5270–7
[20] Bhansali S, Krishnan S, Stefanakos E and Goswami D Y 2010 Tunnel junction based rectenna—a key to ultrahigh efficiency solar/thermal energy conversion *AIP Conf. Proc.* **1313** 79–83
[21] Imafidon O, Georgakopoulos S, Vabbina P K and Pala N 2010 Multifunctional nanodevices for energy harvesting in unconventional spectral ranges *Proc. SPIE* **7679** 76792L
[22] Tien P K and Gordon J P 1963 Multiphoton process observed in the interaction of microwave fields with the tunneling between superconductor films *Phys. Rev.* **129** 647–51
[23] Tucker J R and Feldman M J 1985 Quantum detection at millimeter wavelengths *Rev. Mod. Phys.* **57** 1055–113
[24] Dayem A H and Martin R J 1962 Quantum interaction of microwave radiation with tunneling between superconductors *Phys. Rev. Lett.* **8** 246–8
[25] Tucker J R 1979 Quantum limited detection in tunnel junction mixers *IEEE J. Quantum Electron.* **QE-15** 1234–58
[26] Grover S, Dmitriyeva O, Estes M J and Moddel G 2010 Traveling-Wave metal/insulator/metal diodes for improved infrared bandwidth and efficiency of antenna-coupled rectifiers *IEEE Trans. Nanotechnol.* **9** 716–22
[27] Platero G and Aguado R 2004 Photon-assisted transport in semiconductor nanostructures *Phys. Rep.* **395** 1–157
[28] Kaey B J and Aversa C 1996 Virtual states and photon-assisted tunneling *Phys. Rev.* B **54** R2284–7
[29] Foden C L and Whittaker D M 1998 Quantum electrodynamic treatment of photon-assisted tunneling *Phys. Rev.* B **58** 617–20
[30] Pedersen M H and Büttiker M 1998 Scattering theory of photon-assisted electron transport *Phys. Rev.* B **58** 12993–3006
[31] Tucker J R and Millea M F 1978 Photon detection in nonlinear tunneling devices *Appl. Phys. Lett.* **33** 611–3
[32] Grover S and Moddel G 2012 Engineering the current–voltage characteristics of metal–insulator–metal diodes using double-insulator tunnel barriers *Solid State Electron.* **67** 94–9
[33] Grover S 2011 Diodes for optical rectennas *PhD Thesis* University of Colorado at Boulder, ProQuest, UMI Dissertations Publishing, 2011, 3468381
[34] Joshi S and Moddel G 2013 Efficiency limits of rectenna solar cells: Theory of broadband photon-assisted tunneling *Appl. Phys. Lett.* **102** 083901
[35] Dagenais M, Choi K, Yesilkoy F, Chryssis A N and Peckerar M C 2010 Solar spectrum rectification using nano-antennas and tunneling diodes *Proc. SPIE* **7605** 76050E